Cerebral Cortex, October 2018;28: 3399–3413

doi: 10.1093/cercor/bhx173
Advance Access Publication Date: 18 August 2017
Original Article

ORIGINAL ARTICLE

Loss of TrkB Signaling in Parvalbumin-Expressing Basket Cells Results in Network Activity Disruption and Abnormal Behavior

Dionysios Xenos[1], Marija Kamceva[1], Simone Tomasi[1], Jessica A. Cardin[2,3], Michael L. Schwartz[2] and Flora M. Vaccarino[1,2,3]

[1]Child Study Center, [2]Department of Neuroscience and [3]Kavli Institute for Neuroscience, Yale University School of Medicine, 333 Cedar Street, New Haven, CT 06520, USA

Address correspondence to Flora M. Vaccarino, Yale Child Study Center, Yale University School of Medicine, P.O Box 207900, New Haven, CT 06520, USA. Email: flora.vaccarino@yale.edu

Abstract

The GABAergic system is regulated by the brain-derived neurotrophic factor (BDNF)/Tropomyosin-related kinase B (TrkB) pathway, but the cell-intrinsic role of TrkB signaling in parvalbumin cortical interneuron development and function is unclear. We performed conditional ablation of the TrkB receptor in parvalbumin-expressing (PV) interneurons to study whether postnatal loss of TrkB in parvalbumin cells affects their survival, connectivity, spontaneous and evoked neuronal activity and behavior. Using in vivo recordings of local field potentials, we found reduced gamma oscillations in the sensory cortex of PVcre+; $TrkB^{F/F}$ conditional knockout mice (TrkB cKO), along with increased firing of putative excitatory neurons. There was a significant downregulation in parvalbumin neuron number in cerebral and cerebellar cortices of TrkB cKO mice. In addition, inhibitory synaptic connections between basket cells and pyramidal neurons were profoundly reduced in the neocortex of TrkB cKO mice and there was a loss of cortical volume. TrkB cKO mice also showed profound hyperactivity, stereotypies, motor deficits and learning/memory defects. Our findings demonstrate that the targeting and/or synapse formation of PV-expressing basket cells with principal excitatory neurons require TrkB signaling in parvalbumin cells. Disruption of this signaling has major consequences for parvalbumin interneuron connectivity, network dynamics, cognitive and motor behavior.

Key words: cerebral cortex, GABA interneuron, gamma oscillation, mouse, synapse

Introduction

Interneurons comprise approximately 20% of the neocortical neuronal population and are typically classified according to morphological, neurochemical and electrophysiological properties (DeFelipe et al. 2013). Parvalbumin-containing (PV+) interneurons are unique among interneurons in that they exhibit low input resistance and rapid membrane kinetics, with brief action potentials and minimal spike adaptation, and can sustain very high-frequency firing rates (Petilla Interneuron Nomenclature et al. 2008). Highly interconnected to each other, PV+ interneurons provide strong feedback inhibition to principal (projection) neurons, that is, pyramidal cells in the cerebral cortex and Purkinje neurons in the cerebellum and fast forward inhibition to the striatum. In the cerebral cortex, PV+ cells are about 50% of all GABA interneurons and comprise 2 morphologically and functionally distinct subtypes, the basket cells targeting the soma of pyramidal neurons and the less populous chandelier cells, which target the axon initial segment of excitatory pyramidal cells (DeFelipe et al. 2013). PV interneuron-mediated synaptic inhibition regulates neuronal excitability

(Pouille and Scanziani 2001) and the precise timing of spike generation, playing a key role in generating gamma oscillations, a pattern of network activity associated with cognition (Klausberger and Somogyi 2008; Cardin et al. 2009; Sohal et al. 2009; Yamamoto et al. 2014). In the cerebellum, PV+ basket cells provide an equally powerful inhibitory somatic input to Purkinje neurons. Telencephalic PV+ cortical interneurons are born in the medial ganglionic eminence (MGE) in the ventral telencephalon and subsequently undergo tangential migration into the neocortex (Parnavelas 2000; Marin and Rubenstein 2003), where interneuron precursors mature over the first 2–3 weeks postnatally. In the cerebellum, most GABA interneurons are generated from precursors in the white matter, from where they migrate to the cerebellar cortex in the first week after birth (Grimaldi et al. 2009; Silbereis et al. 2009).

Tropomyosin-related kinase B (TrkB) is the major high-affinity receptor for brain-derived neurotrophic factor (BDNF) and NT4 (Chao 2003) and mediates cell growth and survival, neuronal differentiation and activity-dependent synaptic plasticity in a time- and region-specific manner (Woo and Lu 2006). The biological actions of BDNF/TrkB on excitatory transmission have been extensively characterized (Poo 2001; Lu 2003). However, the role of TrkB receptor signaling in the development and function of GABAergic inhibition has only recently gained attention. In embryonic stages of neuronal development, both BDNF and NT4 regulate the tangential migration of MGE cells into the cortex (Polleux et al. 2002). Postnatally, BDNF and NT4/5 increase the dendritic complexity of hippocampal interneurons (Wirth et al. 2003), and BDNF is involved in the activity-dependent regulation of inhibitory synapse development (Hong et al. 2008; Sakata et al. 2009) as well as in the maturation of PV neurons in the cerebral cortex and olfactory bulb (Berghuis et al. 2006; Itami et al. 2007). These reports have left open the question of how BDNF/TrKB affects the development and functioning of interneurons at the cellular level, and whether interneurons directly require, cell-intrinsically, BDNF/TrKB signaling or whether BDNF acts indirectly upon their development. Recent electrophysiological studies using conditional ablation of the TrkB receptor in PV-expressing cells showed that TrkB is important for gamma-band synchronization in the hippocampal network (Zheng et al. 2011) and for cued fear memory consolidation and extinction (Lucas et al. 2014). However, the role of TrkB in cortical development and cortex-dependent functions has not yet been examined.

Here, we investigated the biological function of the TrkB receptor in the maturation and connectivity of PV+ interneurons over the postnatal period. We found that conditional deletion of the receptor specifically in these neurons beginning in the second postnatal week, after the completion of their migration, decreases the number and disrupts the connectivity patterns of PV+ basket neurons, leading to substantial electrophysiological and behavioral perturbations. Thus, TrkB signaling is of pivotal importance for PV interneuron development and its loss causes specific abnormalities of GABAergic circuitry in vivo with major consequences for motor and cognitive behavior.

Materials and Methods

PV-cre;TrkB$^{WT/F}$ eGFP+ controls and PV-cre; TrkB$^{F/F}$ eGFP+ conditional knockout mice were generated by breeding PV-cre mice (B6;129P2-*Pvalbtm1(cre)Arbr/J*) with mice carrying loxP flanked alleles (Luikart et al. 2003) (a generous gift of Dr. Luis F. Parada, UT Southwestern, Dallas, TX), and CAG-CAT-eGFP reporter mice (Nakamura et al. 2006). All mice used in this study were backcrossed to C57BL/6J mice for at least 10 generations. Animal procedures were approved by the Yale Animal Resources Center and Institutional Animal Care and Use Committee.

Electrophysiological Analysis

For electrophysiology recordings, mice (3–5 months) were anesthetized with isoflurane (0.4–1%) and held in place with a head post cemented to the skull. Both eyes were covered with silicone oil.

All incisions were infiltrated regularly with 1% lidocaine. For visual cortex recordings, a small craniotomy was made over primary visual cortex and electrodes were lowered to a depth of ~200 μm. After a recovery period of 30–60 min, electrode positions were independently adjusted to optimize unit isolation. For striatal recordings, a craniotomy was made over parietal cortex and electrodes were lowered to an initial depth of ~1000 μm. After a recovery period, electrodes were independently lowered into dorsal striatum.

All extracellular single-unit and LFP recordings were made with an array of independently moveable tetrodes mounted in an Eckhorn Microdrive (Thomas Recording). Signals were digitized and recorded by a Digital Lynx system (Neuralynx). All LFP recordings were referenced to the surface of the cortex. Visual stimulation for all recordings was performed using software custom-written in Matlab (The Mathworks) by J. Cardin. Data were sampled at 40 kHz. LFP data were recorded with open filters and single-unit data was filtered from 600–9000 Hz.

Visual stimuli were presented on an LCD monitor at a spatial resolution of 1680 × 1050, a real-time frame rate of 60 Hz, and a mean luminance of 45 cd/m^2 positioned 15 cm from the eye.

Stimuli were generated by custom-written software (J. Cardin, Matlab). Initial hand-mapping was performed to localize the receptive fields of identified cells. To maximize data collection, visual stimuli were positioned to cover as many identified receptive fields as possible. All stimuli were sinusoidal drifting gratings at a temporal frequency of 2 Hz, presented for 1.5 s with an inter-stimulus interval of 2 s.

Unit and LFP analysis used software custom-written in Igor Pro (Wavemetrics) by J. Cardin.

LFP traces were down-sampled to 2 KHz. For each recording site, 20 samples of 5 s duration were used to calculate an average power spectrum. Relative power was calculated by measuring the ratio of power within the frequency band of interest to total power in the power spectrum of the unfiltered LFP. Thresholded unit data was clustered using Klustakwik (Kadir et al. 2014) followed by evaluation in MClust (Schmitzer-Torbert et al. 2005). Only well-isolated units (ID > 18) were included in the analysis. Firing rates were calculated as the average spikes/s over the visual stimulus presentation period or by windowing baseline activity in epochs of equivalent duration.

Spike waveforms of well-isolated regular spiking and fast-spiking cells were characterized by measuring 1) the ratio between the amplitude of the initial peak and the following trough, 2) the duration of the spike at half height, and 3) the timing of spike repolarization to baseline.

We attempted to perform cortical recordings in awake head-fixed animals on a running wheel. However, training of the TrkB cKO mice in the head-fixed paradigm was not possible, due to their motor coordination and learning deficits, and we were unable to obtain recordings.

Immunohistochemistry

Immunohistochemistry was performed in 20 μm thick sections from P48 control and mutant mice. Mice were deeply anesthetized with a single intraperitoneal injection of a ketamine-xylazine cocktail and perfused transcardially with 1× phosphate buffer saline (PBS), followed by 4% paraformaldehyde. Brains were dissected from the skull, post-fixed in the same solution for 24 h, and subsequently placed in a 30% sucrose solution for 24–48 h until equilibration and then frozen. They were then embedded in optimal cutting temperature compound. Serial sagittal 20 μm sections were obtained with a Leica CM1900 cryostat at −20°C. Sections were placed on Superfrost plus glass slides and stored at −80°C until processing. They were washed in 1× PBS and blocked for 1 h in 0.3% Triton-X in PBS containing 5% normal donkey serum.

They were then incubated overnight in blocking solution containing primary antibodies at +4°C and then washed 3 times with PBS. Afterwards, sections were incubated for 1 h in blocking solution containing secondary antibodies at room temperature. They were washed again in PBS and finally with distillated water, and finally mounted and cover slipped using Vectashield mounting medium containing DAPI where applicable (Vector, Burlingame, CA).

Primary antibodies used: rabbit anti-parvalbumin (1:500, SWANT); chicken anti-GFP (1:1000, Abcam); rabbit anti-vGAT (1:1000, Synaptic Systems), guinea pig anti-VGlut1 (1:5000, Millipore); mouse anti-SMI32 (1:1000, Covance); rabbit anti-Gephyrin (1:1000, Abcam); mouse anti-Cre recombinase (1:100, Covance), rabbit anti-TrkB (1:100, Abcam, ab18987)

Stereological Cell Quantification

Cells labeled with parvalbumin and eGFP markers were quantified in 5 serial sagittal sections spanning the entire brain hemisphere in the sagittal plain, spaced 600 μm apart. Four mice per group were analyzed. Cells were identified as positive for a marker if they expressed immunoreactivity visually deemed to be above background, but not if it was very weak. This means that cells exhibiting varying levels of immunolabeling, from only slightly weakly to very strongly immunostained were identified as marker positive. Unbiased stereological cell counting technique was applied using a Zeiss Axioskop 2 Mot Plus fluorescent microscope (Carl Zeiss) connected to a motorized stage controlled by StereoInvestigator 9 software (MicroBrightfield) as previously described from our lab. Contours of the cerebral cortex (excluding the piriform and prelimbic cortices) were delineated at 10× magnification using DAPI stain to delineate reference points. The StereoInvestigator software provided systematic and random sampling of cell counts using the optical fractionator workflow method. Contours of the cerebral cortex (excluding the piriform and prelimbic cortices), dorsal striatum, globus pallidus and cerebellar molecular layer (excluding the Purkinje cells) were delineated at 10× magnification using DAPI stain for anatomical orientation according to precise reference points. Cells were counted at 40× magnification using a 3D counting frame in a sampling grid. Further technical information is described in a recent article published from our lab (Komitova et al. 2013). Two-way Factorial ANOVA was applied to test significance, using GraphPad Prism 6 software, with genotype as dependent variable and PV and eGFP data as categorical predictors (independent factors) for each of the 4 brain areas analyzed. Sidak's multiple comparisons test was applied to test possible interactions between independent factors.

Image Acquisition and Analysis

Quantification of the intensity levels of presynaptic vGlut1+ and vGAT+ terminal boutons in individual cells was performed on images of either PV/eGFP/vGlut1 or SMI32/eGFP/vGAT immunostained brain sections from PVcre;TrkB$^{WT/WT}$ or PVcre; TrkB$^{F/F}$ P48 mouse brains. Four mice per group were analyzed. We examined 2 sections per mouse, each of which provided at least 3 cells to analyze, for a total number of 24 cells per group. Stacks of images spanning 9 μm in the z-plane were taken in the various areas to be analyzed: 1) layer V of the primary motor (M1) cortex; 2) the Purkinje layer of the cerebellar cortex; 3) the overall area of the deep cerebellar nuclei identified by expression of SMI32+ staining; and 4) the cell sparse area closest to the pial surface as Layer 1 and pyramidal shaped cells immediately underneath as Layer 2. Puncta analysis and fluorescence intensity measurements were done with a 100× objective on a Zeiss Observer Z1 microscope equipped with an ApoTome 2. Exposure time was kept at the same levels for all the images (300 ms for vGlut1, 200 ms for vGAT, 500 ms for eGFP, 70 ms for TrkB, and 1000 ms for Gephyrin). A maximum projection image was created from each stack using the Zeiss Axiovision 4.8 software. Both SMI32+ and PV+/eGFP+ cells in layer V were manually traced using the Adobe Photoshop software (version CS5). For the reconstruction of the deep cerebellar nuclei SMI32+ area, photo composites were created from the single images and subsequently the areas were manually traced by using the same software. The intensity of vGAT, vGLUT1, and TrkB expression was determined using ImageJ 1.44c software (National Institutes of Health). The intensity of immunolabeling corrected for background signal was determined using the following formula: "Corrected Total Cell Fluorescence = Integrated Density − (Area of selected cell × Mean fluorescence of background)". Acquisition of separate cut view files from the final images confirmed the presence of the synaptic boutons onto the actual soma of traced cells by visual colocalization of immunolabeling markers in all 3 dimensions. For puncta analysis of single vGAT, eGFP, and Gephyrin puncta, as well as colocalized clusters (eGFP+ and Gephyrin+), each pyramidal cell was traced using SMI32+ cell body area contour, and the total number of puncta was obtained using the "puncta analysis" plugin of the same software at fixed thresholds of fluorescent detection and divided by each cell body area, so as to obtain data of puncta density per cell surface. About 30–35 cells were estimated per group. For estimation of puncta in cortical layers, density of puncta was estimated in a counting frame box measuring 29.5 × 42 μm randomly chosen within the cortical layer analyzed. Student's *t*-test was used to test significance between controls and TrkB mutant mice.

Behavioral Analyses

All animal procedures were approved by the local ethical committee (IACUC) and met the guidelines of the local and American regulations and the Standards for Use of Laboratory Animals (NIH). Mice were housed in standard cages and water and standard rodent chow were available ad lib. Behavioral experiments were conducted during the light phase of the light/dark cycle, and in some cases performed by trained observers blind to genotype.

For behavioral examination we used different batteries of tests to capture specific phenotypes.

In pilot experiments, we tested mice lacking a single TrkB allele (PVcre+; TrkB$^{F/WT}$) and mice that lacked Cre recombinase

activity (PVcre–; $TrkB^{F/WT}$ or PVcre–; $TrkB^{F/F}$) and found no significant behavioral differences between these 2 groups and that of wild-type C57/B6 mice. Hence, in all subsequent experiments, data from these 2 strains were lumped together and both considered as controls. Male and female PVcre+; $TrkB^{F/F}$ KO mice and age matched controls (PVcre–; $TrkB^{F/F}$ and PVcre+; $TrkB^{F/WT}$) were subjected to the open-field test to assess locomotor activity, the Lashley III maze for spatial and working memory, video recording of motor activity for quantification of stereotypic movements, and gait analysis for limb coordination.

Open-Field Activity

Spontaneous open-field behavior was evaluated in mice from both PV-TrkB knockouts (KO) and wild-type (WT) groups at P90. KO ($n = 13$) and WT ($n = 21$) mice tested were placed in a

Plexiglas enclosed open field (44 × 44 × 8 cm) equipped with infrared photo beams coupled to a computer running TruScan software (Coulbourn Instruments, Whitehall, PA) to automatically record both horizontal and vertical movements within the field. Locomotion was measured by a pair of infrared light-beam sensors located on each side of the enclosure at a height of 2 cm.

Sensors were spaced 6.5 cm from each end, so that the light beams formed a matrix of 3 × 3 squares over the surface. A locomotor activity count was recorded each time a mouse crossed the full distance (at least 6.5 cm) between 2 beams. Activity was monitored during a single 60-min session and measures of total distance moved, center distance, the average velocity of movements, rest time, center time and jumps exceeding 1 inch above the floor plane were recorded.

Rotarod

Motor learning was measured by the accelerating rotarod task on 3 consecutive days, for 6 trials per day (AccuRotor, AccuScan Instruments, Columbus, OH). KO ($n = 13$) and WT ($n = 21$) mice were placed on a rotating rod at the slowest speed, at 0.1 RPM, and accelerated at a constant rate of acceleration, either 1.0 RPM/s. rate of acceleration (fast acceleration) or 0.1 RPM/s. (slow acceleration). Acceleration time was 200 s. The latency of each trial was measured as the time the mouse stayed on the rod until it either fell off of the rotating rod, or clung to the rod without running for an entire revolution. All animals were tested on 6 spaced sessions in a single day in order to evaluate motor coordination and learning.

Gait Analysis

All animals were habituated for 5 min before testing. Paw print analysis was performed on all KO ($n = 13$) and WT ($n = 21$) mice. The test consisted of a single section per animal. Paws were dipped in washable non-toxic paint. The testing chamber was a plexiglass box (12 × 180 × 30 cm) containing a start chamber (12 × 12 × 12 cm), a corridor containing the footprint paper and the goal chamber. Wall dividers ensured the mouse moved properly towards the goal chamber. A distinct and detailed paw image of the footprints on the paper (5 × 150 cm) was obtained. Illumination of the testing enclosure was critical to obtaining an optimal contrast between the paws and body of the mouse. Gait pattern parameters that were considered in this analysis included: “stride length”, as the distance between the center of the plantar of the forefoot and the hind-foot plantar, on the same side of the body within the same stride; “forepaw base and hind-paw base”, as a lateral measure of the distance between the front paws or the hind paws, indicative of the degree of lateral displacement of limbs when the feet are in contact with the ground; “right or left overlap”, as the distance between the center of the plantar of the front paw and the corresponding hind-foot measured in successive strides, considering that when rodents walk in a straight line, the hind-foot on one side of the body is placed close to the same place where the forefoot was placed. One-tailed Student’s *t*-test was used to evaluate significance between experimental groups.

Video Recordings

At the end of the open-field test, animals were put in a glass cylinder (8 inches high, 6 inches wide) using the same lighting conditions and 2 video cameras were placed above and on the side of the box. Animals were subjected to live video recording for 5 min simultaneously from the 2 cameras. The 3-min central time of the videos were scored by an observer who did not participate to any of the experiments and was blind to the genotype. The total number and direction of 360° rotations in the horizontal plane and the total number of upward head movements in the vertical plane were scored. One-tailed *t*-test was used to test significance between experimental groups.

Lashley III Maze

The Lashley III maze is designed to assess learning and memory in mice without aversive motivators such as food and water restriction or stressors such as swimming. Mice quickly adapt exploring the maze, and are motivated to traverse the maze for the reward of returning to their familiar home cage. The start box, maze arms, and goal box are modular to allow for cleaning and modifiability of the maze. The walls of the start box, maze arms, and goal box are constructed of black Plexiglas to eliminate visual cues from outside and inside the maze. Maze arms are 45 cm long, 7 cm high and 5 cm wide. Doors leading to consecutive arms of the maze are 4 × 4 cm and are situated 11 cm from the outer walls of the maze. The goal box is 19.5 cm long × 7 cm high × 5 cm wide. The start box is 8 × 9.5 × 7 cm. Separate clear Plexiglas pieces are placed on top of the start box, maze, and goal box to allow visualization of each mouse as it progresses through the maze while preventing mice from escaping. During the testing period mice are individually housed. The test was performed once a day for up to 15 days for each animal. Each mouse was placed in the start box and allowed to traverse the maze until it reached the goal box. The task of the mouse was to exit the start box, run down alley 1 to the door, turn right into alley 2, then left into alley 3, right into alley 4, and left into the goal box.

The task was considered completed only when the animal was finally able to reach its home cage and its total body was completely inside. Errors were defined as a deviation from this optimal path and could be due to an entry into a cul-de-sac at the end of an alley or retracing its path towards the start box. Errors were also defined as the whole body passing a line perpendicular to either edge of a door. Thus, running past the door of alley 1 and then retracing towards the start box, again missing the alley door, would count as 2 errors. Re-entering the start box would count as a further error. An animal was considered to have reached criterion performance if the total errors on 2 consecutive days of testing had been 1 or less. Failure to reach criterion within the 15 days of testing was considered a failure to learn and testing was stopped.

Statistical Analyses

Statistical analyses were performed using Statistica 7 and GraphPad Prism 6 softwares. We used Student's *t*-test to test significance when only 2 groups were compared (controls vs. mutants), 2-way factorial ANOVA when interaction of more than 2 independent variables were examined onto the same 2 experimental groups, 2-way repeated measures ANOVA when groups were compared across time (open field), and a Kaplan–Meier cumulative proportion survival/failure time analysis for the Lashley III experiment using the SPSS software.

Values were considered significant when $P < 0.05$. Fisher LSD and Sidak post-hoc analyses were conducted when *P* values reached significance. Data are presented as mean ± SEM.

Results

Specificity and Distribution of Cre Recombination Driven by PV-Cre Mice

To examine the impact of BDNF/TrkB signaling on the cell-intrinsic development and function of PV-expressing cells, we conditionally deleted the TrkB receptor only in PV^+ interneurons using PV-Cre mice carrying $TrkB^{F/F}$ alleles. A Cre recombination reporter, CAG-CT-eGFP (Nakamura et al. 2006) was used to estimate the specificity and sensitivity of the TrkB deletion. In both cortex and striatum, between 90% and 100% of the $eGFP^+$ cells also expressed PV in both PVcre+; $TrkB^{F/F}$ conditional knockout (here and after TrkB cKO) and PVcre+; $TrkB^{WT/WT}$ control mice, suggesting that the TrkB recombination was highly specific for the PV^+ cells (Fig. 1*A*). However, the apparent efficiency of Cre recombination as detected by the reported expression in PV neurons differed between regions. For example, 67–73% of the PV+ cortical neurons were also eGFP+ (Fig. 1*B*) and virtually all cerebellar Purkinje cells were also eGFP+ (Fig. 1*D–F*), whereas no eGFP was detected in the cerebellar molecular layer interneurons and only 16–24% of PV+ neurons in the caudate/putamen were eGFP+ (Fig. 1*B*). Cre immunostaining confirmed that Cre was not highly expressed in the basal ganglia, however Cre was expressed by cerebellar neurons (presumably interneurons) in the molecular layer, suggesting that there was widespread TrkB deletion in these cells despite no reporter expression (Fig. 1*C–E*).

To ensure that TrkB inactivation had occurred in the targeted cells, we quantified fluorescence intensity of the TrkB immunostaining onto the soma of eGFP+ PV+ cortical interneurons. We found a profound loss of TrkB expression in the eGFP+ parvalbumin cells in the neocortex of the TrkB cKO mice ($P < 0.001$) as compared with their control counterparts (Supplementary Fig. 1).

Because of the low efficiency of TrkB recombination in basal ganglia, we focused on PV phenotypes in cortex and cerebellum.

Decreased Neocortical High-Frequency Activity Following Deletion of TrkB from PV Interneurons

To determine the functional impact of TrkB deletion from PV interneurons on spontaneous and sensory-evoked network activity in the intact brain, we made tetrode recordings from primary visual cortex (V1) and dorsal striatum of anesthetized mutants and controls. TrkB cKO animals demonstrated enhanced sensitivity to isoflurane anesthesia, and we therefore used a slightly lower level of anesthetic in mutants than in controls (controls: 0.81 ± 0.09% isoflurane, $n = 4$; mutants: 0.52 ± 0.04% isoflurane,

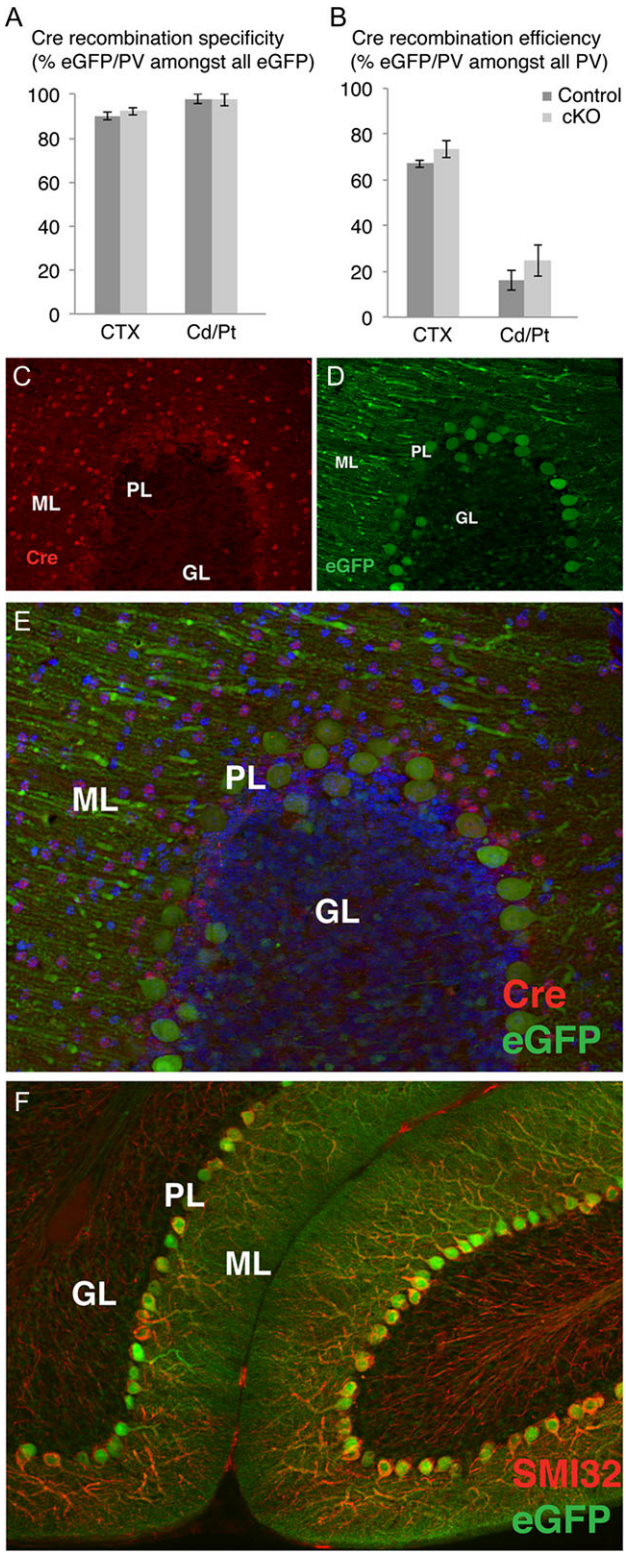

Figure 1. Analysis of Cre recombination and reporter expression across brain regions in controls and TrkB cKO mice. (*A*,*B*) Cre recombination specificity and efficiency as determined by eGFP/PV double immunostaining in different brain regions. (*C–E*), Cre recombinase (*C*) and eGFP (*D*) immunohistochemistry and merged image (*E*) in cerebellar cortex in a control animal, showing that cerebellar molecular layer interneurons express Cre even though they lack eGFP reporter expression; (*F*) Virtually all Purkinje cells, labeled by SMI32+, express the eGFP reporter.

$n = 5$; $P < 0.05$, Mann–Whitney U-test). Depth of anesthesia was matched across groups by maintaining the animals in a state where the cortical slow oscillation was observed at a consistent frequency (controls: 0.40 ± 0.08 Hz, $n = 4$; mutants: 0.40 ± 0.09 Hz, $n = 5$; $P > 0.05$, Mann–Whitney U-test).

TrkB cKO animals demonstrated reduced spontaneous high-frequency local field potential (LFP) power in the visual cortex and a concomitant shift towards low frequencies (<10 Hz) (Fig. 2A).

Both spontaneous and visually evoked activity in the gamma (30–50 Hz) range was significantly reduced in the TrkB cKO animals ($n = 4$ control and 5 mutant animals; $P < 0.05$ in both cases; Fig. 2B). In association with the observed changes in LFP activity, we also found increased firing of cortical regular spiking (RS), putative excitatory neurons in TrkB cKO animals under spontaneous ($n = 25$ control and 20 mutant RS cells; $P < 0.01$, Mann–Whitney U-test), but not visually driven ($P > 0.05$, Mann–Whitney U-test) conditions (Fig. 2C).

In contrast, and consistent with low recombination efficiency in striatal interneurons, no firing rate alterations were observed ($n = 18$ control and 23 mutant cells; $P > 0.05$, Mann–Whitney U-test; Fig. 2D) in the dorsal striatum of the mutants. However, striatal LFP power was reduced in the gamma band ($n = 3$ control and 3 mutant animals; $P < 0.05$, Mann–Whitney U-test; not shown), likely because field potential activity in the striatum is heavily driven by cortical afferents. Together, these data suggest that TrkB deletion from PV+ interneurons leads to dysregulation of patterned activity in the cortex and concomitant disinhibition of local excitatory neurons.

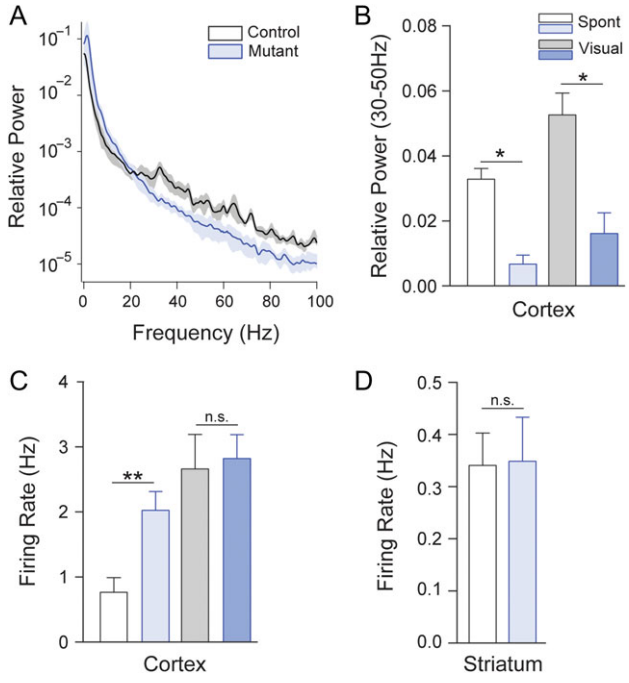

Figure 2. Deficits in high-frequency activity in cortex following trkb deletion from PV+ interneurons. (A) LFP Population average power spectra of spontaneous LFP activity in primary visual cortex of control (black) and mutant (blue) animals. (B) Mutants showed a significant deficit in gamma band (30–50 Hz) during both spontaneous and sensory-evoked activity. (C) Elevated spontaneous, but not visually evoked, firing rates in regular spiking (RS), putative excitatory neurons in visual cortex of mutants. (D) TrkB cKO mutants showed no significant change in striatal firing rates.

Cellular Mechanisms by which TrkB Regulates Neuronal Activity in PV$^+$ Interneurons

We next explored the cellular mechanisms by which the loss of the TrkB gene product in PV interneurons caused a decrease in gamma-band oscillations in the cortex and a simultaneous increase in spontaneous firing of excitatory cortical neurons. Possible reasons could include a downregulation of the activity-dependent protein parvalbumin, which would suggest a defective maturation of fast-spiking interneurons, as well as abnormalities in their connectivity pattern with pyramidal cells.

To assess whether the absence of TrkB signaling resulted in a general loss of PV neurons and/or decrease in PV expression, we quantified the numbers of eGFP reporter and PV immunoreactive cells in young adult (P48) control and TrkB cKO mice in the cerebral and cerebellar cortices. In the cerebral cortex, 2-way factorial ANOVA revealed a main effect of genotype [$F(1,12) = 23.33$, $P < 0.001$]; Sidak's multiple comparisons test showed a statistically significant decrease in both the number of PV ($P < 0.01$) and eGFP ($P < 0.05$) immunoreactive cells in TrkB cKO mice as compared to controls (Fig. 3B–I). Consistently with these changes, we found that cortical volume was 62.3 ± 2.8 mm^3 in the TrkB cKO mice as compared to 78.8 ± 5.2 mm^3 in controls, revealing a statistically significant 21% decrease in mutant mice ($n = 4$, $P < 0.05$) (Fig. 3A). In the cerebellar cortex, we found a significant decrease in the PV-expressing basket cell number in the molecular layer of the TrkB cKO mice, compared to their control counterparts. (Fig. 4A,B,D). Low eGFP reporter gene recombination in these cells prevented us from detecting an accurate estimation of eGFP+ cell number differences. Lastly, we detected a trend towards a decrease of the molecular layer volume in the TrkB cKO mice compared to control animals (17.1 3 ± 1.45 mm^3 in controls vs. 13.5 ± 0.9 mm^3 in the TrkB cKO mice, $n = 5$, $P = 0.07$, Student's t-test) (Fig. 4C).

In order to know whether TrkB signaling is also required for the formation or maintenance of synaptic connections of PV cells with principal neurons, we assessed inhibitory synapses of PV+ basket interneurons impinging onto the soma of cortical pyramidal cells in layer V and layers II–III of motor cortex, identified by SMI32 neurofilament immunolabeling. Comparison of the corrected total cell fluorescence of the vGAT immunostaining onto SMI32+ pyramidal neuron cell bodies between controls and TrkB cKO mice revealed a significant decrease of vGAT axon terminals in the TrkB cKO mice ($P < 0.01$, student's t-test, mean ± SEM controls = 66.98 ± 9.2, cKO = 19.6 ± 1.2, data not shown). To corroborate these findings, we analyzed the actual number of vGAT+ puncta impinging onto SMI32+ pyramidal cells, normalized by cell area. The density of presynaptic inhibitory VGAT+ terminal bouton immunoreactivity onto the somata of layer V pyramidal cells was profoundly decreased in the neocortex of TrkB cKO mice compared to their control counterparts ($P < 0.01$) (Fig. 5A–D,I). A similar decrease ($n = 4$, $P < 0.05$) was observed in the density of eGFP+ boutons on the somata of layer V motor cortex pyramidal cells (Fig. 5E,F,J), consistent with the notion of decreased inhibitory input onto layer V pyramidal cells from PV+ interneurons. These data suggest that basket cells lacking TrkB send fewer inhibitory synapses onto the cell body of primary motor cortex layer V pyramidal neurons. We next examined whether the loss of presynaptic inhibitory axon terminals was paralleled by corresponding changes in the postsynaptic compartment. We found a statistically significant reduction in density of postsynaptic Gephyrin immunoreactive puncta ($P < 0.05$) as well as eGFP+/Gephyrin+ colocalized clusters onto SMI32+ cortical layer V pyramidal

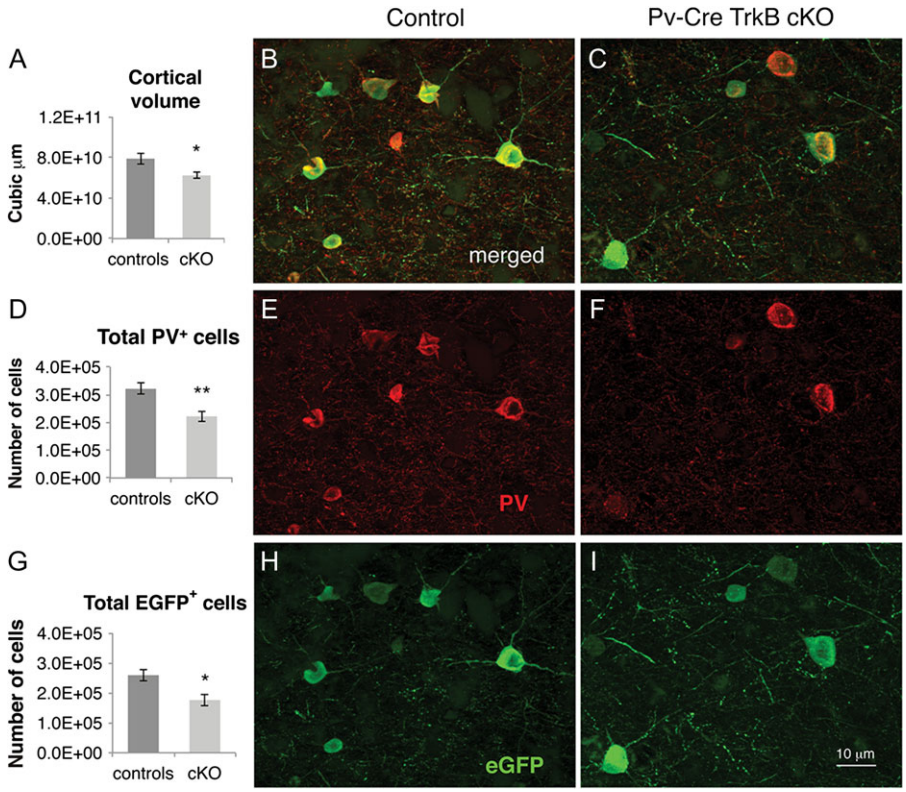

Figure 3. Neocortical volume deficit and decreased PV+/eGFP+ immunoreactivity in TrkB cKO mice. (*A*) Stereological analyses showed a 21% decrease in volume in the neocortex in TrkB cKO mice at P48vs as compared to control animals, *$P < 0.05$, Student's *t*-test. (*B–I*) PV/eGFP double immunohistochemistry in the neocortex of controls and mutant mice at P48. Stereological quantification showed a significant decrease in the total number of PV+ cortical interneurons (*D*) and in the total number of eGFP+ cells (*G*). *$P < 0.05$; **$P < 0.01$ by Sidak's multiple comparisons test in 2-way factorial ANOVA. $N = 4$ mice/group. Scale bar: 10 μm.

neurons ($n = 4$ mice per group, $P < 0.01$, 2-tailed *t*-test, Fig. 5*E,F,J*). A similar decrease in density of eGFP+ presynaptic terminals, postsynaptic Gephyrin immunoreactive puncta and eGFP +/Gephyrin+ colocalized clusters was detected in in cortical layer layer II/III pyramidal neurons (Fig. 5*G,H,K*). To investigate whether the lack of the TrkB receptor in PV cells disrupts excitatory inputs, we quantified the corrected total cell fluorescence of the vGluT1 immunostaining onto the soma of PV+/eGFP+ cells in layer IV/V of primary motor cortex. The amount of vGluT1+ fluorescence did not differ between the 2 experimental groups ($n = 3$, mean ± SEM controls: 40.5 ± 6.3, cKO = 43.2 ± 8, data not shown).

Together, these data suggest that PV+ basket cells in TrkB cKO mice deliver fewer inhibitory terminals onto layer V and layer II/III pyramidal cells, but receive a normal number of somatic excitatory synapses. We therefore conclude that the TrkB receptor plays a role within PV+ interneurons in either axon guidance or synapse formation onto cortical pyramidal neurons, whereas it appears to be dispensable for the formation of excitatory synaptic terminals onto PV cells.

In order to compare changes in cortical and cerebellar circuitry, we quantified the density of vGAT+ terminal bouton immunoreactivity onto Purkinje cells and onto cells of the deep cerebellar nuclei. As shown in Figure 6*A–D,I*, there was no statistically significant change in the density of presynaptic inhibitory vGAT+ terminal bouton immunoreactivity onto the cell body of Purkinje cells between groups, suggesting no apparent loss of inhibitory inputs from molecular layer basket interneurons onto Purkinje cells. Lastly, the density of the vGAT+ terminal bouton immunoreactivity in the deep cerebellar nuclei, identified by SMI32 staining, also did not differ between the two experimental groups (Fig. 6*E–H,J*).

TrkB Receptor Deletion in PV-Expressing Cells Results in Severe Hyperlocomotion, Impaired Motor Coordination and Increased Motor Stereotypies

We next investigated whether the decrease in basket cell connectivity with principal neurons and the associated changes in the pattern of functional activity resulted in behavioral abnormalities. Hence, we tested these mice for behavioral deficits in the motor (locomotion, coordination, stereotypies) and cognitive (spatial and working memory) domains.

The distance traveled by the TrkB cKO mice over the 1-h testing period was significantly greater than that of controls. TrkB cKO mice also demonstrated a progressive increase in locomotion over the initial 30 min of testing compared to a small decrease for control mice (Fig. 7A). A repeated measures 2-way ANOVA showed a main effect of genotype for total distance traveled [$F(1,30) = 8.1$, $P < 0.01$] and a significant interaction between genotype and time [$F(11,330) = 2.02$, $P < 0.05$]. No main effect of gender was observed in this analysis. The distance traveled for TrkB cKO mice in the central 70% of the open field was also significantly greater than control mice with a main effect of genotype [$F(1,30) = 9.8$, $P < 0.01$] and a significant interaction between genotype and time [$F(11,330) = 2.5$, $P < 0.01$] (Fig. 7*B*), suggesting a decreased level of anxiety and greater exploration compared to controls. Similarly, the velocity of movement (cm/min) increased during the 1-h testing period for TrkB cKO mice compared to controls (Fig. 7*C*) [main effect of

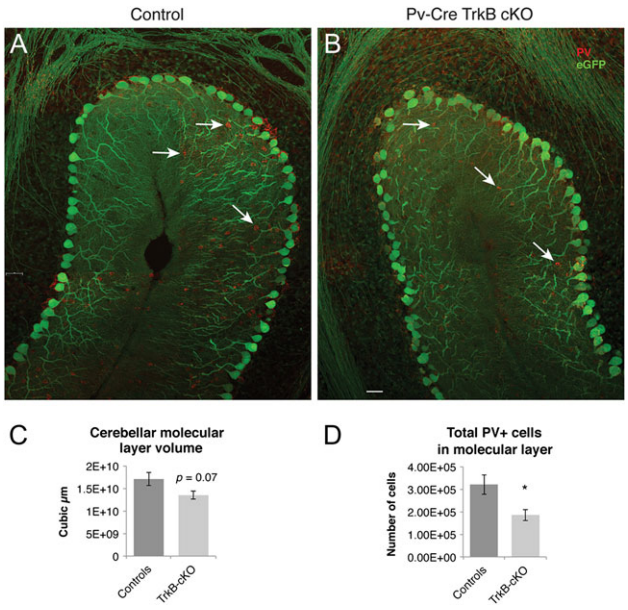

Figure 4. Decrease in PV+/eGFP+ immunoreactivity and cerebellar molecular layer volume in TrkB cKO mice. (*A*,*B*) PV/eGFP double immunohistochemistry in the cerebellar cortex of controls and mutant mice at P48. The arrows indicate PV-expressing basket cells in the molecular layer. (*C*) Stereological quantification of the volume of the cerebellar molecular layer of controls and mutant mice showing a strong trend towards a decrease in TrkB cKO mice ($P = 0.07$, $N = 5$ mice/group). (*D*) Stereological quantification of the total number of PV+ cerebellar interneurons showed a significant decrease in the total number of PV+ basket cells in the TrkB cKO mice. *$P < 0.05$, Student's *t*-test, $N = 5$ mice/group.

genotype, $F(1,30) = 7.86$, $P < 0.01$; genotype × time interaction, $F(11,330) = 2.07$, $P < 0.05$], suggesting that an increase in the velocity of movement contributed to the greater distance traveled by the TrkB cKO mice. Lastly, TrkB cKO mice exhibited an increased number of jumps, approaching significance ($P = 0.06$, data not shown). Taken together, these data show that TrkB cKO mice exhibit an increased velocity of movement and hyperactivity that are maintained over the 60-min test session.

Next, the performance of TrkB cKO mice was assessed using an accelerating Rotarod task to explore potential alterations in motor coordination. Control mice demonstrated improved performance in the amount of time they were able to stay on the rotating rod across testing sessions in a single day, averaging 9.1 s on the first of 6 sessions and increasing to 15.2 s by the sixth session. In contrast, the majority of TrkB cKO mice fell from the rotating rod immediately on placement onto the rod. The average time for the TrkB cKO mice on the first of 6 sessions was 0.1 s and increased only to 0.4 s by the sixth session.

These results (data not shown) suggest that the TrkB cKO mice suffer from a severe deficit in motor coordination.

To assay whether the defective motor coordination of the TrkB cKO mice was paralleled by abnormalities in their gait pattern, we performed a gait analysis experiment. Animals (4–5 months old) walked the length of a 5 × 50 cm corridor and footprint patterns of control and TrkB cKO mice were compared (Fig.7*D*,*E*). Control mice walked in a straight line, with a regular alternating gait, placing the hind-paw precisely at the position where the ipsilateral forepaw had been in the previous step. As shown in Figure 7*D*,*E*, conditional knockout mice displayed significantly shorter stride lengths compared to control mice for

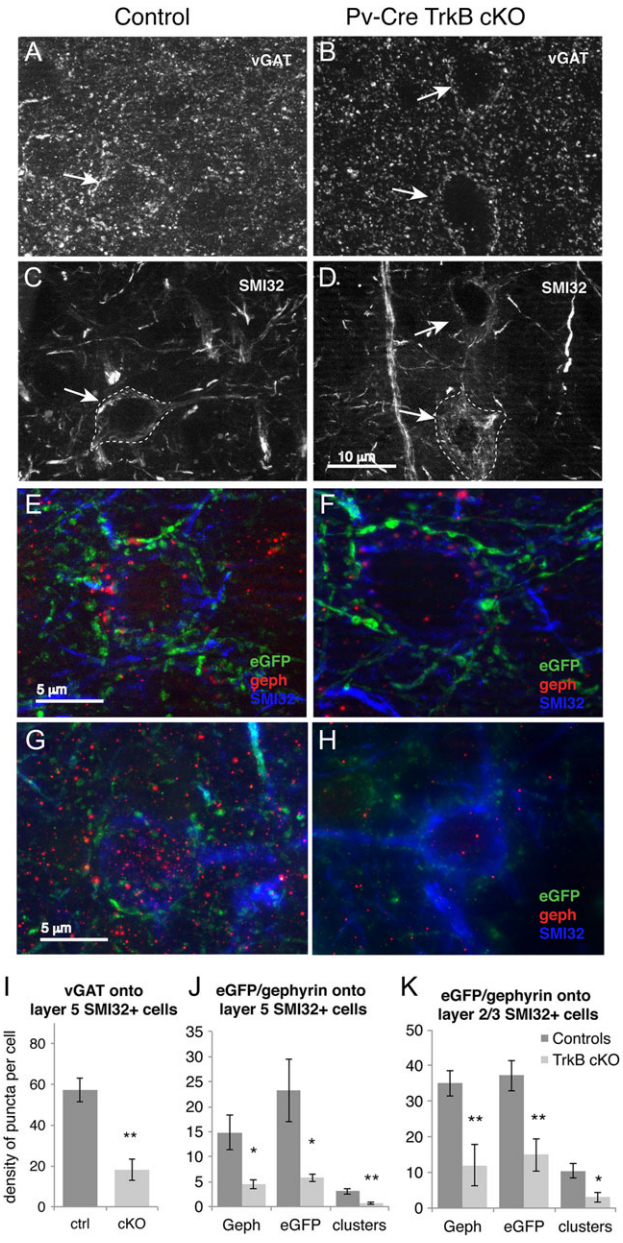

Figure 5. Cortical layer V pyramidal cells in TrkB cKO mice receive fewer inhibitory inputs from basket cells. (*A*,*B*) vGAT immunohistochemistry and (*C*,*D*) SMI32 immunohistochemistry showing the traced cell bodies of layer V pyramidal neurons (arrows) in controls and mutant mice at P48. (*E*,*F*) Merged images of eGFP (green), Gephyrin (red), and SMI32 (blue) showing layer V pyramidal neurons and their PV neuron input (labeled by GFP) in controls and mutant mice at P48. (*G*,*H*) Merged images of eGFP (green), Gephyrin (red), and SMI32 (blue) showing layer II/III pyramidal neurons and their PV neuron input (labeled by GFP) in controls and mutant mice at P48.For quantification purposes, all fluorescent images were acquired using equal time exposure. (*I*) Quantification of vGAT+ terminal bouton density onto SMI32+ cortical layer V excitatory neurons in motor cortex showing a decrease in TrkB cKO mice. **$P < 0.01$, Student's *t*-test. $N = 4$ ctrl and 5 cKO mice/group. (*J*) Quantification of presynaptic (eGFP+) and postsynaptic (Gephyrin+) puncta density as well as colocalized cluster density onto SMI32+ pyramidal neurons bodies in layer V showing a significant downregulation in the TrkB cKO at P48. *$P < 0.05$ and **$P < 0.01$, Student's *t*-test. $N = 4$ mice per group. (*K*) Quantification of presynaptic (eGFP+) and postsynaptic (Gephyrin+) puncta density as well as colocalized cluster density onto SMI32+ pyramidal neurons bodies in layer II/III showing a significant downregulation in the TrkB cKO. *$P < 0.05$ and **$P < 0.01$, Student's *t*-test. $N = 4$ mice per group.

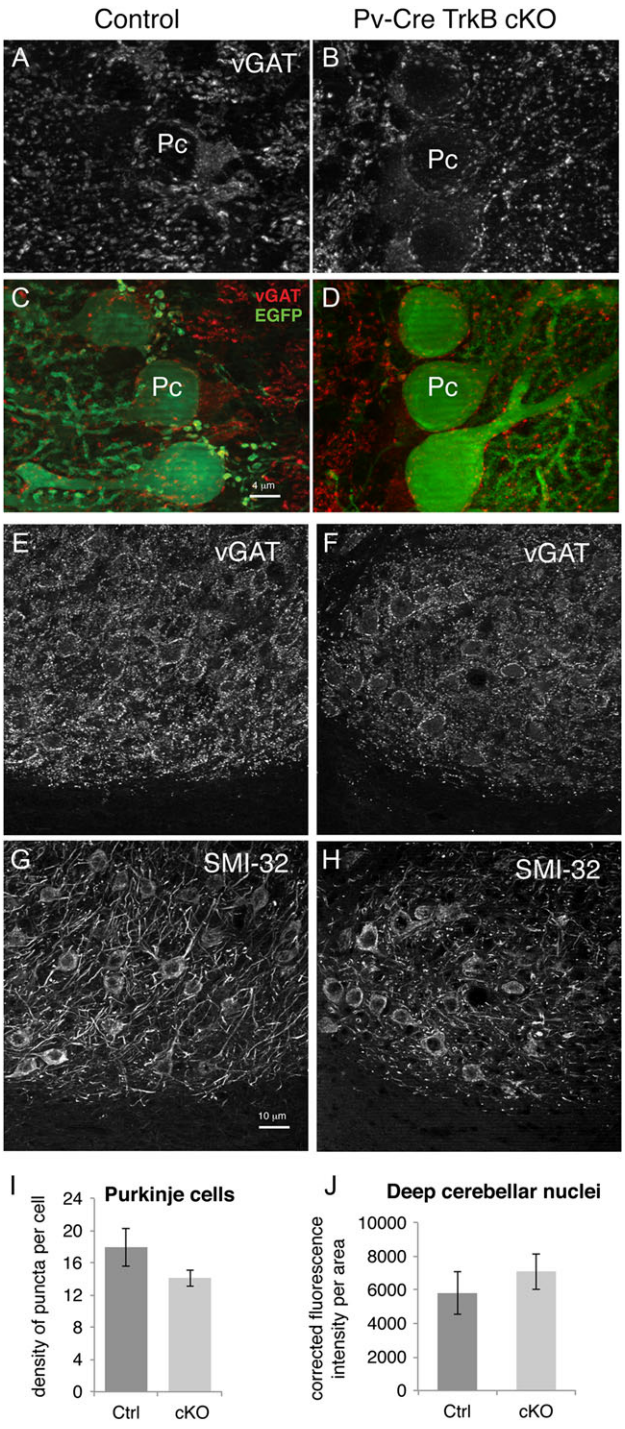

Figure 6. Cerebellar Purkinje cells in the TrkB cKO mice receive normal inhibitory inputs from basket cells, and extend normal amount of afferents in the deep cerebellar nuclei. (*A*,*B*) vGAT immunohistochemistry in cerebellar cortex of control and mutant mice at P48. (*C*,*D*) Merged images of vGAT (red) and eGFP immunohistochemistry showing cerebellar Purkinje cell bodies (green) and their inhibitory afferents (red). Pc: Purkinje cell. (*E*,*F*) vGAT immunohistochemistry and (*G*,*H*) SMI32 immunohistochemistry showing excitatory neurons and their inhibitory afferents in the deep cerebellar nuclear complex in control and mutant mice. (*I*) Quantification of vGAT puncta density onto eGFP+ Purkinje cells show no significant decrease in TrkB cKO mice at P48. $N = 5$ mice/group. (*J*) Quantification of corrected total cell fluorescence intensity of vGAT+ terminal boutons onto the deep cerebellar nuclear complex showed no significant difference between experimental groups. $N = 3$ ctrl and 4 cKO mice/group. Scale bar, 4 μm in *A*–*D* and 10 μm in *E*–*H*.

both fore and hind limbs on both sides, as well as an almost ($P = 0.053$) significantly increased distance between front and hind footprint placement (overlap) on the right side. No significant differences were found for the limb base widths (Fig. 7*D*,*E*), suggesting that the degree of lateral displacement of limbs when the paws are in contact with the ground was not significantly affected. In conclusion, we show that TrkB deletion in PV cells caused ataxia characterized by shorter, unevenly spaced strides and non-uniform step alternation on the left side. General motor strength, as assessed by their ability to grip and hold onto the cage top, did not seem to be affected.

Observation of TrkB conditional knockout mice revealed the presence of repetitive movements, characterized by stereotypic motor jerks of the head and excessive repetitive grooming (Movie 1), as well as fast turning movements of the body in a single preferred direction (Movie 1). In order to quantify differences in stereotypic movements between control and cKO mice, we analyzed the middle 3 min of each 5-min video recordings comparing mice of both groups, after placing them in a new glass cylinder. We scored each video for the total number of upward head movements and for the total number of 360° turning movements. Our analysis revealed that the total number of upward head movements was significantly higher in the TrkB cKO mice (33.3 ± 5.1 movements) compared to their controls (9.45 ± 1.8 movements $P < 0.001$, Fig. 8*A*, Movie 1).

There was also an increased number of turning movements for the conditional knockout mice (124.4 ± 33.2) compared to the controls (40.9 ± 6.7 movements, $P < 0.01$, Fig. 8*B*) (Movie 1).

Further, the number of turning movements in the animals' preferred direction was significantly increased in the conditional knockout mice (87 ± 22.7) compared to their control counterparts (24.1 ± 3.9 movements, $P < 0.01$, Fig. 8*C*), which highlighted the highly stereotypic component of their motor hyperactivity.

Deficit in Learning and Memory in TrkB cKO Mice

In order to assess potential deficits in neocortical functions in TrkB cKO mice, we examined spatial learning and memory abilities using the Lashley III maze. The choice of the Lashley III maze test was motivated by a previous pilot experiment using the Morris Water maze paradigm in which TrkB cKO mice were found to be unable to swim. Like the Water maze, the Lashley III maze task also assesses spatial learning and memory. In this task, animals must remember a sequence of leftright spatial choices while navigating between the start and goal chambers of the maze.

Memory for the correct sequence of these choices across test days is determined by assessing the number of errors in navigating the maze until a criterion performance of 2 successive days with 1 or less errors is attained. Both the control and TrkB cKO mice had similar latencies for exiting the starting box to initiate the task (data not shown). A Kaplan–Meier cumulative proportion survival/failure time analysis was used to compare the curves for days to criteria and failure rates for TrkB cKO and control mice. Based upon this analysis, TrkB cKO mice required significantly more days to reach criterion than did control mice ($P < 0.001$). Indeed, none of the TrkB cKO mice achieved criterion performance before the 15 day cut-off for testing (Fig. 8*D*). In addition, TrkB cKO mice had a significantly greater number of incorrect arm entries (557.6 ± 99.3 errors) compared to the controls (70.6 ± 14.4 errors, $P < 0.001$) (Fig. 8*E*).

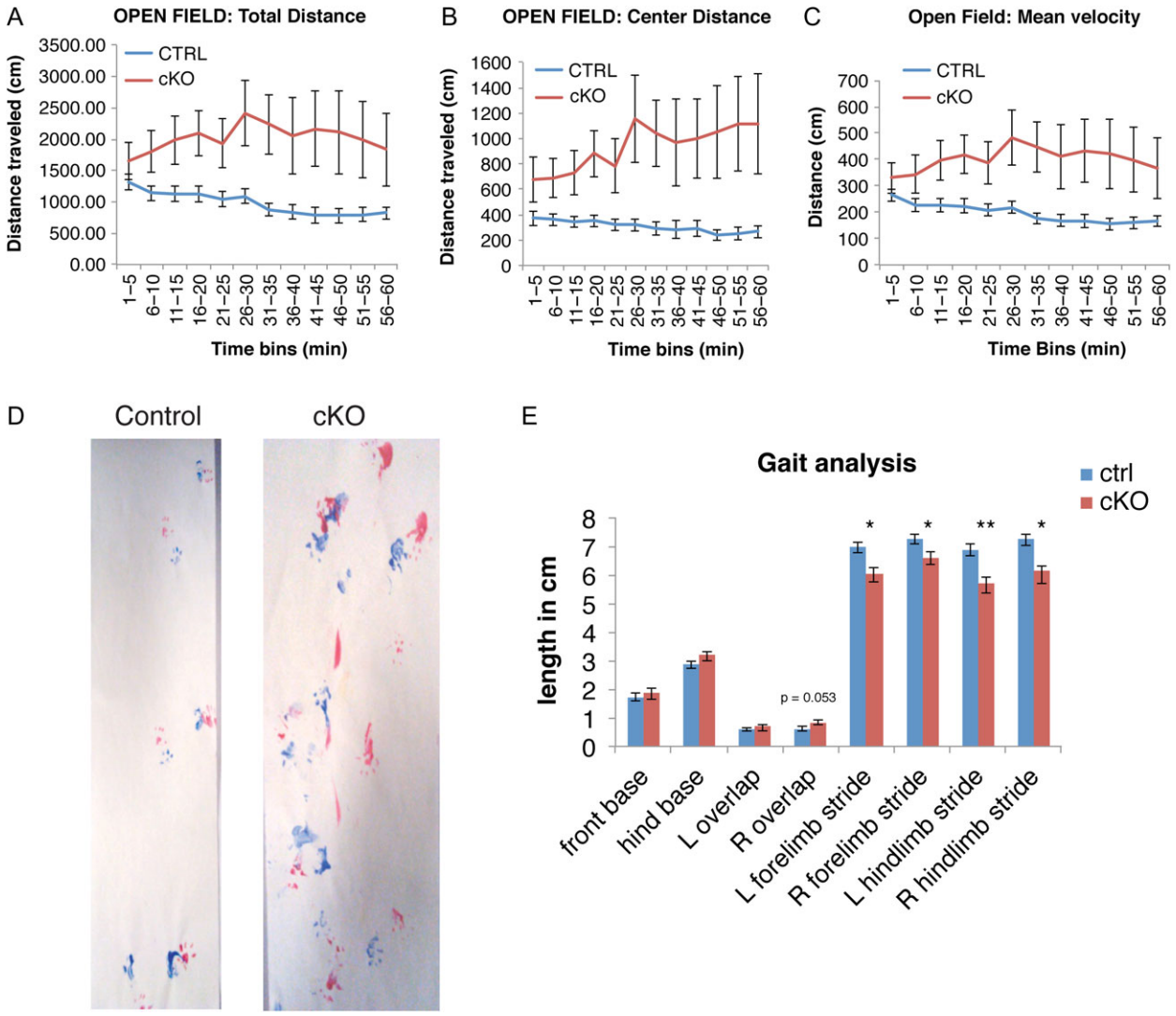

Figure 7. TrkB deletion from PV+ interneurons caused pronounced hyperactivity and abnormal gait patterns. Locomotor activity in open field of control ($N = 21$) and mutant ($N = 13$) 3-month-old mice. Total distance traveled (A), and distance traveled in the central 70% of the field (B) was significantly greater in the TrkB cKO mice compared to controls. Mean velocity (C) was also significantly higher in TrkB cKO mice. Repeated measures 2-way ANOVA and Fisher LSD post-hoc test. (D,E) Gait analysis in control ($N = 22$) and mutant ($N = 13$) 4-month-old mice. Footprints (D) of both control and knockouts (red: forelimb, blue: hindlimb) and (E) gait analysis parameters tested: stride length, right and left overlap and front and hind base measurements. R: right, L: left. *$P < 0.05$ and **$P < 0.01$, 2-tailed Student's t-test.

Lastly, TrkB cKO mice required an overall greater time to complete the task, exit the maze and reach the goal/home cage (Fig. 8F). Together, the results are consistent with a working memory and spatial memory defects.

Discussion

We have demonstrated a pivotal role of the TrkB neurotrophin receptor in the development of PV^+ cortical basket cells. Conditional ablation of the TrkB receptor from PV-expressing cells causes a small but significant decrease in the number of PV+ fast-spiking interneurons in both the cerebral and the cerebellar cortices, as well as severe defects in PV+ basket cells axon targeting leading to a significant loss of inhibitory synapses onto principal neurons of the cerebral cortex. This in turn is associated with decreased cortical oscillations in the gamma range with increased activity of putative pyramidal neurons. Loss of TrkB in PV cells also results in abnormal behavioral phenotypes at both the motor and cognitive levels, consistent with the known role of gamma-band activity in synchronizing and coordinating the activity of cortical neuron assemblies. This reiterates the crucial role PV+ GABAergic inhibitory interneurons in the regulation of neuronal excitation and network functioning. It has previously been reported that disruption of GABAergic circuitry is associated with various developmental neuropsychiatric disorders, including intellectual disability (Cramer et al. 2010), schizophrenia (Lewis et al. 2005; Gonzalez-Burgos et al. 2011; Sullivan and O'Donnell 2012) and Tourette syndrome (Kalanithi et al. 2005; Kataoka et al. 2010). Significant decreases in TrkB transcripts (Hashimoto et al. 2005; Hashimoto and Lewis 2006) and TrkB protein levels in the blood (Hung and Huang 2013) have been detected in patients with schizophrenia. Indeed, our model recapitulates several pathophysiological features of these developmental psychiatric disorders.

BDNF signaling enhances the development of GABAergic inhibitory neurons and induces the expression of related proteins, including Gad67/Gad1 and parvalbumin (Jones et al. 1994; Alcantara et al. 1997; Huang et al. 1999). In addition, in transgenic

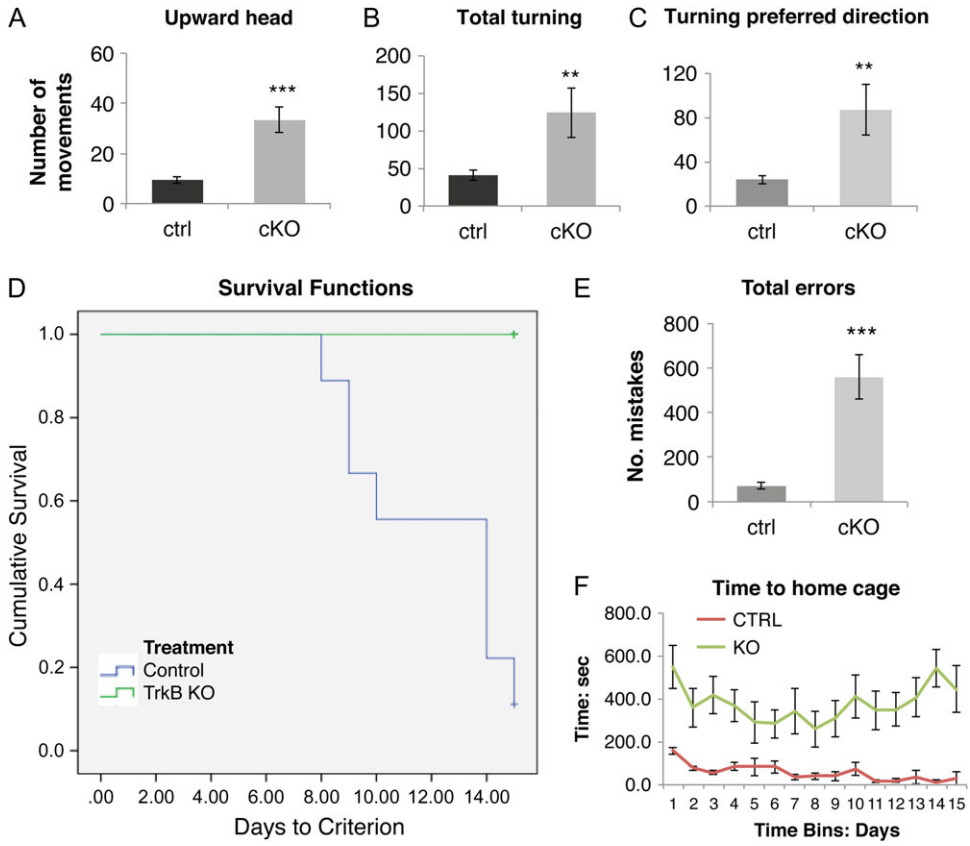

Figure 8. TrkB conditional knockouts showed increased stereotypic behavior and learning/memory deficits. (*A–C*) 5-min video recordings in horizontal and vertical planes of free locomotor behavior of control ($N = 11$) and mutant ($N = 10$) 3-month-old mice. Total number of upward head movements in the vertical plane (*A*), spin-like movements in the horizontal plane in both left and right directions (*B*) and in the animals' preferred direction (*C*) were significantly increased in the TrkB knockout mice. $^{**}P < 0.01$ and $^{***}P < 0.001$, 1-tailed Student's *t*-test. (*D–F*) Lashley III maze analysis test for spatial memory in control ($N = 9$) and mutant ($N = 10$) 5-month-old mice. (*D*) Graph of results of the Lashley III test for spatial memory for control (green line) and TrkB cKO mice (blue line). Graph lines indicate the proportion (vertical axis) of animals within each group failing to reach criterion performance (1 or 0 errors over 2 successive days of testing) vs. the number of days needed to reach criterion (horizontal axis). None of the knockout mice reached criteria performance on the Lashley III maze task compared to all the control mice. Comparison of groups using the Kaplan–Meier cumulative proportion survival/failure time analysis (SPSS software) indicated a significant difference between the groups ($P < 0.001$). (*E*) Errors evaluation in Lashley III maze. $^{***}P < 0.001$, 2-tailed Student's *t*-test. (*F*) Time to home cage: repeated measures 2-way ANOVA and Fisher LSD post-hoc: $P < 0.001$.

mice overexpressing BDNF, the maturation of GABAergic interneurons (Aguado et al. 2003) and particularly of PV-expressing interneurons (Huang et al. 1999) was accelerated. We demonstrate that the loss of TrkB results in a decrease in PV+ neuron number in the cerebral cortex and cerebellum. The parallel decrease in PV and eGFP is consistent with an actual loss of PV cells, rather than an effect of TrkB on PV gene expression, because eGFP is expressed earlier than PV protein, and once genetically induced, reporter gene expression should be stably marking the PV neuron lineage. However we cannot discriminate whether BDNF/TrkB impairs PV neuron maturation at earlier stages of development or their survival. Another possibility is that decreased PV cell number is attributable to altered migration, although we consider this unlikely, since cortical PV neuron migration occurs prenatally and in the first postnatal week, and is completed by the time the eGFP gene becomes active at P12. Overall, our results demonstrate a direct, cell-intrinsic requirement for the TrkB receptor signaling for PV neuron development/survival in vivo which is consistent with the known survival-promoting effect of BDNF on PV+ neurons (Jones et al. 1994). The severe synaptic loss can be attributed in part to the decreased number of PV-expressing cortical interneurons in TrkB cKO mice, and/or to an independent role of TrKB on the maturation of basket cell terminals, resulting in an overall decreased number of inhibitory synapses on the cell body of cortical pyramidal cells. This is demonstrated by the decreased vGAT+ presynaptic terminals, the loss of eGFP+ boutons derived from PV+ interneurons on pyramidal cell bodies, the decreased number of Gephyrin+ postsynaptic terminals, as well as the loss of colocalized eGFP +/Gephyrin+ clusters on pyramidal cell bodies in the cerebral cortex of TrKB cKO mice. The analysis likely excluded the chandelier PV+ cells, as PV-expressing chandelier cells synapse on the axon initial segment of excitatory neurons; therefore, we cannot exclude that a similar synaptic defect also exists in chandelier cells. To our knowledge this is the first report of a synaptic defect of basket cells caused by deficient TrkB signaling in cortical PV neurons. The data are consistent with previous literature suggesting that neurotrophin ligands generally promote synaptic development, synaptic vesicle exocytosis, and neurotransmitter release (Rutherford et al. 1997; Vicario-Abejon et al. 1998; Seil and Drake-Baumann 2000; Baldelli et al. 2002; Carmona et al. 2003). Moreover, neurotrophin signaling through TrkB is crucial for clustering and localization of GABAergic synapses (Chen et al. 2011; Wuchter et al. 2012). PV interneurons play a key role in maintaining the balance of excitation and inhibition in cortical networks (Shu et al. 2003; Haider et al. 2006; Xue et al. 2014).

Feed-forward inhibition from these interneurons also contributes to the temporal precision of cortical activity by restricting the window of opportunity for postsynaptic spine generation (Pouille and Scanziani 2001). Precisely timed PV inhibition is critical in the generation of gamma-band oscillations, a temporal pattern of activity thought to be important for information encoding (Csicsvari et al. 2003; Cardin et al. 2009; Sohal et al. 2009) and theta oscillations, which may play a role in spatial navigation (Buzsaki and Eidelberg 1983; Marshall et al. 2002; Royer et al. 2012). Consistent with the decreased number of basket-pyramidal cell synaptic connections, the conditional deletion of TrkB from PV-expressing interneurons was associated with a loss of gamma-band LFP activity in vivo, indicating a functional disruption of the ability of PV inhibition to entrain local excitatory neurons. Concomitantly, there was a shift of spontaneous oscillations towards lower frequencies. We also observed enhanced spontaneous firing of putative excitatory neurons, suggesting disinhibition of pyramidal cells and a consequent disruption of the excitatory-inhibitory balance in the cortical network. Our finding of increased spontaneous firing of cortical excitatory cells in TrkB cKO mice suggests a lack of significant homeostatic changes compensating for the dysregulated excitatory-inhibitory balance in the cortical network, consistently with the lack of significant differences in the number of excitatory vGLUT1+ terminal contacts onto the cell body of PV+ cortical interneurons. The loss of gamma-band power was also observed in hippocampal slice recordings from PV-Cre TrkB cKO mice (Zheng et al. 2011).

Defective inhibitory targeting of principal neurons of the cortex and accompanying network dysfunction was associated with abnormal motor and cognitive behavior. Our mutant mice had spontaneous hyperlocomotion and spontaneous stereotypic behaviors, characterized by circling movements in a preferred direction, as previously reported (Lucas et al. 2014), as well as repetitive upward head movements combined with grooming. This is also consistent with previous studies showing that BDNF heterozygous null mutants (Kernie et al. 2000) and CaMKII-Cre; $BDNF^{F/F}$ cKO mice (Rios et al. 2001) exhibit locomotor hyperactivity. Stereotypic motor disorders have been linked to striatal dysfunctions in a number of dyskinesias including Tourette syndrome, Parkinson's and Huntington's disease. Disturbances in corticostriatal synapses in Huntington's disease have been linked to impairment of postsynaptic plasticity (Plotkin et al. 2014), imbalance of p75/TrkB protein expression (Brito et al. 2013), and altered huntingtin-dependent TrKB trafficking and subcellular localization (Liot et al. 2013).

In our model, very little Cre recombination was detected in the striatum, and indeed we found no decrease in PV cell number, size and arborization in this region (data not shown). Consistently, no electrophysiological abnormality was detected in the striatum. Prior data have shown that an almost identical pattern of hyperlocomotion with stereotypic circling behavior was seen in mice with loss of pyramidal cells in layer V within frontotemporal cortex (Shin et al. 2004). Cortical abnormalities such as thinning and abnormal functional activity have been detected in Tourette syndrome (Peterson et al. 1998; Sowell et al. 2008) and reduced expression of the TrkB receptor was also reported not only in the striatum but also in the motor cortex of individuals with Huntington's disease (Gines et al. 2006). This seems to suggest that stereotypic behavior and hyperactivity can also be associated with aberrant cortical function. Cortical pyramidal neurons project to striatal PV interneurons and to medium spiny neuron (MSN) in the basal ganglia, modulating their activity. Previous work using simultaneous recording from multiple striatal and cortical locations in awake animals demonstrated that dorsolateral striatal PV neurons are entrained by cortical high-voltage spindle oscillations and ventral/medial striatal neurons are entrained by hippocampal theta rhythm (Berke et al. 2004). Hence decreased gamma power activity in cortex in our PVCreTrkB mutants will likely cause decreased gamma activity in the striatum, consistent with our observation of reduced striatal LFP power in the gamma band in our mutant animals. It has also been shown that PV interneuron-driven, gamma power striatal activity preferentially inhibits MSN of the direct pathway (Gittis et al. 2010). One consequence of decreased cortical gamma-band modulation would then be hyperactivity of direct pathway MSNs, which is known to result in hyperlocomotion and stereotypic movements (Albin et al. 1989) as observed in our TrkB cKO animals.

The TrkB mutant mice also showed severe ataxia. This behavioral phenotype is likely attributable to dysfunctional cerebellar circuitry, although the number of vGAT+ presynaptic inhibitory axon terminals impinging onto Purkinje cells were not significantly downregulated in the TrkB cKO mice. Both TrkB and TrkC are expressed in the cerebellum, including Purkinje cells, granular and molecular layers (Segal et al. 1995; Johnson et al. 2007; Sherrard et al. 2009). However, the relative expression of these receptors changes during development: TrkB is higher prenatally and decreases after birth, whereas TrkC remains constant, such that the ratio between TrkB/TrkC mRNA changes from 5:1 in the first week to 1.2 in the adult cerebellum (Segal et al. 1995; Wullner et al. 1998). Both these receptors play a role in axonal growth (Segal et al. 1995), suggesting that there could be partial redundancy over later stages of postnatal development. Nonetheless, our cellular analysis revealed a significant decrease in the total number of PV-expressing basket cells in the cerebellar molecular layer and a trend towards a volume loss of the cerebellar molecular layer in the Trkb cKO mice. This cellular defect is likely to have an impact in the organization and function of the cerebellar circuitry explaining the ataxia and abnormal motor coordination.

Pertinent to the role of TrkB in cortical function, we detected prominent cognitive abnormalities in TrkB cKO mice, which have not been previously reported. The cognitive component of the behavioral deficits was characterized by severe and long-lasting spatial learning and working memory deficits. During the 15 days of Lashley III maze testing, TrkB cKO mice had a greater number of errors in traversing the maze and were unable to meet criterion performance. Furthermore, mutant mice failed to show learning improvement over time. These abnormalities could be attributed to the general role of BDNF/TrkB signaling in promoting synaptic plasticity and LTP-dependent learning and memory consolidation (Minichiello 2009; Lu et al. 2014). However, since the conditional deletion of TrkB signaling involved only parvalbumin neurons and not pyramidal cells, we believe that the more likely neurobiological substrate for the memory abnormalities is the specific loss of cortical gamma-band activity, likely attributable to decreased input of basket cells to pyramidal cell somata, which secondarily would alter the temporal precision of cortical activity (Cardin et al. 2009; Sohal et al. 2009). Hippocampal network dysfunction is also likely to contribute to the spatial memory defect in these mice (Zheng et al. 2011).

In conclusion, our results suggest that TrkB signaling plays a critical role in the proper anatomical and functional integration of PV-expressing basket cells into the local circuitry, as the lack of TrkB precludes the formation of a normal number of basket cells-principal cell synapses in cortex. The defect in PV

interneuron circuit formation and function is sufficient to cause permanent alterations in motor and cognitive behavior. TrkB is likely required for normal formation of PV interneuron connections during the critical period, when PV cells begin to express PV and display their fast-spiking properties. Interestingly, these deficits are not compensated over time. We suggest that this is a driving mechanism for the known dysfunction in interneuron maturation and connectivity found in some neuropsychiatric disorders where both BDNF/TrkB levels and cortical GABA interneuron signaling may be reduced, which include bipolar disorder and schizophrenia (Guidotti et al. 2000; Volk et al. 2000, 2001; Ray et al. 2014) as well as in disorders with aberrant corticostriatal synaptic plasticity, such as Tourette syndrome and Hungtington's disease.

Supplementary Material

Supplementary data is available at *Cerebral Cortex* online.

Funding

This work was supported by the National Institutes of Health (P01 NS062686 to FMV, R01 EY022951 to JAC).

Notes

We thank Luis F. Parada (UT Southwestern, Dallas, TX) for the gift of a $TrkB^{F/F}$ mice. We thank Rachael Couture, Sarah Collica, Jessica Mariani, and Mariangela Amenduni for excellent technical assistance. We also thank Hanna E. Stevens for help with statistical analyses and stimulating discussions and Soraya Scuderi for crucial help with puncta analysis. *Conflict of Interest*: The authors declare no competing financial interests.

References

Aguado F, Carmona MA, Pozas E, Aguilo A, Martinez-Guijarro FJ, Alcantara S, Borrell V, Yuste R, Ibanez CF, Soriano E. 2003. BDNF regulates spontaneous correlated activity at early developmental stages by increasing synaptogenesis and expression of the K+/Cl- co-transporter KCC2. Development. 130:1267–1280.

Albin RL, Young AB, Penney JB. 1989. The functional anatomy of basal ganglia disorders. TINS. 12:366–375.

Alcantara S, Frisen J, del Rio JA, Soriano E, Barbacid M, Silos-Santiago I. 1997. TrkB signaling is required for postnatal survival of CNS neurons and protects hippocampal and motor neurons from axotomy-induced cell death. J Neurosci. 17: 3623–3633.

Baldelli P, Novara M, Carabelli V, Hernandez-Guijo JM, Carbone E. 2002. BDNF up-regulates evoked GABAergic transmission in developing hippocampus by potentiating presynaptic N- and P/Q-type Ca2+ channels signalling. Eur J Neurosci. 16: 2297–2310.

Berghuis P, Agerman K, Dobszay MB, Minichiello L, Harkany T, Ernfors P. 2006. Brain-derived neurotrophic factor selectively regulates dendritogenesis of parvalbumin-containing interneurons in the main olfactory bulb through the PLCgamma pathway. J Neurobiol. 66:1437–1451.

Berke JD, Okatan M, Skurski J, Eichenbaum HB. 2004. Oscillatory entrainment of striatal neurons in freely moving rats. Neuron. 43:883–896.

Brito V, Puigdellivol M, Giralt A, del Toro D, Alberch J, Gines S. 2013. Imbalance of p75(NTR)/TrkB protein expression in Huntington's disease: implication for neuroprotective therapies. Cell Death Dis. 4:e595.

Buzsaki G, Eidelberg E. 1983. Phase relations of hippocampal projection cells and interneurons to theta activity in the anesthetized rat. Brain Res. 266:334–339.

Cardin JA, Carlen M, Meletis K, Knoblich U, Zhang F, Deisseroth K, Tsai LH, Moore CI. 2009. Driving fast-spiking cells induces gamma rhythm and controls sensory responses. Nature. 459: 663–667.

Carmona MA, Martinez A, Soler A, Blasi J, Soriano E, Aguado F. 2003. Ca(2+)-evoked synaptic transmission and neurotransmitter receptor levels are impaired in the forebrain of trkb (–/–) mice. Mol Cell Neurosci. 22:210–226.

Chao MV. 2003. Neurotrophins and their receptors: a convergence point for many signalling pathways. Nat Rev Neurosci. 4:299–309.

Chen AI, Nguyen CN, Copenhagen DR, Badurek S, Minichiello L, Ranscht B, Reichardt LF. 2011. TrkB (tropomyosin-related kinase B) controls the assembly and maintenance of GABAergic synapses in the cerebellar cortex. J Neurosci. 31: 2769–2780.

Cramer NP, Best TK, Stoffel M, Siarey RJ, Galdzicki Z. 2010. GABAB-GIRK2-mediated signaling in Down syndrome. Adv Pharmacol. 58:397–426.

Csicsvari J, Jamieson B, Wise KD, Buzsaki G. 2003. Mechanisms of gamma oscillations in the hippocampus of the behaving rat. Neuron. 37:311–322.

DeFelipe J, Lopez-Cruz PL, Benavides-Piccione R, Bielza C, Larranaga P, Anderson S, Burkhalter A, Cauli B, Fairen A, Feldmeyer D, et al. 2013. New insights into the classification and nomenclature of cortical GABAergic interneurons. Nat Rev Neurosci. 14:202–216.

Gines S, Bosch M, Marco S, Gavalda N, Diaz-Hernandez M, Lucas JJ, Canals JM, Alberch J. 2006. Reduced expression of the TrkB receptor in Huntington's disease mouse models and in human brain. Eur J Neurosci. 23:649–658.

Gittis AH, Nelson AB, Thwin MT, Palop JJ, Kreitzer AC. 2010. Distinct roles of GABAergic interneurons in the regulation of striatal output pathways. J Neurosci. 30:2223–2234.

Gonzalez-Burgos G, Fish KN, Lewis DA. 2011. GABA neuron alterations, cortical circuit dysfunction and cognitive deficits in schizophrenia. Neural Plast. 2011:723184.

Grimaldi P, Parras C, Guillemot F, Rossi F, Wassef M. 2009. Origins and control of the differentiation of inhibitory interneurons and glia in the cerebellum. Dev Biol. 328:422–433.

Guidotti A, Auta J, Davis JM, Di-Giorgi-Gerevini V, Dwivedi Y, Grayson DR, Impagnatiello F, Pandey G, Pesold C, Sharma R, et al. 2000. Decrease in reelin and glutamic acid decarboxylase67 (GAD67) expression in schizophrenia and bipolar disorder: a postmortem brain study. Arch Gen Psychiatry. 57: 1061–1069.

Haider B, Duque A, Hasenstaub AR, McCormick DA. 2006. Neocortical network activity in vivo is generated through a dynamic balance of excitation and inhibition. J Neurosci. 26: 4535–4545.

Hashimoto T, Bergen SE, Nguyen QL, Xu B, Monteggia LM, Pierri JN, Sun Z, Sampson AR, Lewis DA. 2005. Relationship of brain-derived neurotrophic factor and its receptor TrkB to altered inhibitory prefrontal circuitry in schizophrenia. J Neurosci. 25:372–383.

Hashimoto T, Lewis DA. 2006. BDNF Val66Met polymorphism and GAD67 mRNA expression in the prefrontal cortex of subjects with schizophrenia. Am J Psychiatry. 163: 534–537.

Hong EJ, McCord AE, Greenberg ME. 2008. A biological function for the neuronal activity-dependent component of BDNF transcription in the development of cortical inhibition. Neuron. 60:610–624.

Huang ZJ, Kirkwood A, Pizzorusso T, Porciatti V, Morales B, Bear MF, Maffei L, Tonegawa S. 1999. BDNF regulates the maturation of inhibition and the critical period of plasticity in mouse visual cortex. Cell. 98:739–755.

Hung YY, Huang TL. 2013. Lower serum tropomyosin receptor kinase B levels in patients with schizophrenia. Biomed J. 36: 132–136.

Itami C, Kimura F, Nakamura S. 2007. Brain-derived neurotrophic factor regulates the maturation of layer 4 fast-spiking cells after the second postnatal week in the developing barrel cortex. J Neurosci. 27:2241–2252.

Johnson EM, Craig ET, Yeh HH. 2007. TrkB is necessary for pruning at the climbing fibre-Purkinje cell synapse in the developing murine cerebellum. J Physiol. 582:629–646.

Jones KR, Farinas I, Backus C, Reichardt LF. 1994. Targeted disruption of the BDNF gene perturbs brain and sensory neuron development but not motor neuron development. Cell. 76: 989–999.

Kadir SN, Goodman DF, Harris KD. 2014. High-dimensional cluster analysis with the masked EM algorithm. Neural Comput. 26:2379–2394.

Kalanithi PS, Zheng W, Kataoka Y, DiFiglia M, Grantz H, Saper CB, Schwartz ML, Leckman JF, Vaccarino FM. 2005. Altered parvalbumin-positive neuron distribution in basal ganglia of individuals with Tourette syndrome. Proc Natl Acad Sci USA. 102:13307–13312.

Kataoka Y, Kalanithi PS, Grantz H, Schwartz ML, Saper C, Leckman JF, Vaccarino FM. 2010. Decreased number of parvalbumin and cholinergic interneurons in the striatum of individuals with Tourette syndrome. J Comp Neurol. 518: 277–291.

Kernie SG, Liebl DJ, Parada LF. 2000. BDNF regulates eating behavior and locomotor activity in mice. EMBO J. 19: 1290–1300.

Klausberger T, Somogyi P. 2008. Neuronal diversity and temporal dynamics: the unity of hippocampal circuit operations. Science. 321:53–57.

Komitova M, Xenos D, Salmaso N, Tran KM, Brand T, Schwartz ML, Ment L, Vaccarino FM. 2013. Hypoxia-induced developmental delays of inhibitory interneurons are reversed by environmental enrichment in the postnatal mouse forebrain. J Neurosci. 33:13375–13387.

Lewis DA, Hashimoto T, Volk DW. 2005. Cortical inhibitory neurons and schizophrenia. Nat Rev Neurosci. 6:312–324.

Liot G, Zala D, Pla P, Mottet G, Piel M, Saudou F. 2013. Mutant Huntingtin alters retrograde transport of TrkB receptors in striatal dendrites. J Neurosci. 33:6298–6309.

Lu B. 2003. Pro-region of neurotrophins: role in synaptic modulation. Neuron. 39:735–738.

Lu B, Nagappan G, Lu Y. 2014. BDNF and synaptic plasticity, cognitive function, and dysfunction. Handb Exp Pharmacol. 220:223–250.

Lucas EK, Jegarl A, Clem RL. 2014. Mice lacking TrkB in parvalbumin-positive cells exhibit sexually dimorphic behavioral phenotypes. Behav Brain Res. 274:219–225.

Luikart BW, Nef S, Shipman T, Parada LF. 2003. In vivo role of truncated trkB receptors during sensory ganglion neurogenesis. Neuroscience. 117:847–858.

Marin O, Rubenstein JL. 2003. Cell migration in the forebrain. Annu Rev Neurosci. 26:441–483.

Marshall L, Henze DA, Hirase H, Leinekugel X, Dragoi G, Buzsaki G. 2002. Hippocampal pyramidal cell-interneuron spike transmission is frequency dependent and responsible for place modulation of interneuron discharge. J Neurosci. 22:RC197.

Minichiello L. 2009. TrkB signalling pathways in LTP and learning. Nat Rev Neurosci. 10:850–860.

Nakamura T, Colbert MC, Robbins J. 2006. Neural crest cells retain multipotential characteristics in the developing valves and label the cardiac conduction system. Circ Res. 98:1547–1554.

Parnavelas JG. 2000. The origin and migration of cortical neurones: new vistas. Trends Neurosci. 23:126–131.

Peterson BS, Skudlarski P, Anderson AW, Zhang H, Gatenby JC, Lacadie CM, Leckman JF, Gore JC. 1998. A functional magnetic resonance imaging study of tic suppression in Tourette syndrome. Arch Gen Psychiatry. 55:326–333.

Petilla Interneuron Nomenclature Group, Ascoli GA, Alonso-Nanclares L, Anderson SA, Barrionuevo G, Benavides-Piccione R, Burkhalter A, Buzsaki G, Cauli B, Defelipe J, Fairen A, et al. 2008. Petilla terminology: nomenclature of features of GABAergic interneurons of the cerebral cortex. Nat Rev Neurosci. 9:557–568.

Plotkin JL, Day M, Peterson JD, Xie Z, Kress GJ, Rafalovich I, Kondapalli J, Gertler TS, Flajolet M, Greengard P, et al. 2014. Impaired TrkB receptor signaling underlies corticostriatal dysfunction in Huntington's disease. Neuron. 83:178–188.

Polleux F, Whitford KL, Dijkhuizen PA, Vitalis T, Ghosh A. 2002. Control of cortical interneuron migration by neurotrophins and PI3-kinase signaling. Development. 129:3147–3160.

Poo MM. 2001. Neurotrophins as synaptic modulators. Nat Rev Neurosci. 2:24–32.

Pouille F, Scanziani M. 2001. Enforcement of temporal fidelity in pyramidal cells by somatic feed-forward inhibition. Science. 293:1159–1163.

Ray MT, Shannon Weickert C, Webster MJ. 2014. Decreased BDNF and TrkB mRNA expression in multiple cortical areas of patients with schizophrenia and mood disorders. Transl Psychiatry. 4:e389.

Rios M, Fan G, Fekete C, Kelly J, Bates B, Kuehn R, Lechan RM, Jaenisch R. 2001. Conditional deletion of brain-derived neurotrophic factor in the postnatal brain leads to obesity and hyperactivity. Mol Endocrinol. 15:1748–1757.

Royer S, Zemelman BV, Losonczy A, Kim J, Chance F, Magee JC, Buzsaki G. 2012. Control of timing, rate and bursts of hippocampal place cells by dendritic and somatic inhibition. Nat Neurosci. 15:769–775.

Rutherford LC, DeWan A, Lauer HM, Turrigiano GG. 1997. Brain-derived neurotrophic factor mediates the activity-dependent regulation of inhibition in neocortical cultures. J Neurosci. 17:4527–4535.

Sakata K, Woo NH, Martinowich K, Greene JS, Schloesser RJ, Shen L, Lu B. 2009. Critical role of promoter IV-driven BDNF transcription in GABAergic transmission and synaptic plasticity in the prefrontal cortex. Proc Natl Acad Sci USA. 106: 5942–5947.

Schmitzer-Torbert N, Jackson J, Henze D, Harris K, Redish AD. 2005. Quantitative measures of cluster quality for use in extracellular recordings. Neuroscience. 131:1–11.

Segal RA, Pomeroy SL, Stiles CD. 1995. Axonal growth and fasciculation linked to differential expression of BDNF and NT3 receptors in developing cerebellar granule cells. J Neurosci. 15:4970–4981.

Seil FJ, Drake-Baumann R. 2000. TrkB receptor ligands promote activity-dependent inhibitory synaptogenesis. J Neurosci. 20:5367–5373.

Sherrard RM, Dixon KJ, Bakouche J, Rodger J, Lemaigre-Dubreuil Y, Mariani J. 2009. Differential expression of TrkB isoforms switches climbing fiber-Purkinje cell synaptogenesis to selective synapse elimination. Dev Neurobiol. 69:647–662.

Shin DM, Korada S, Raballo R, Shashikant CS, Simeone A, Taylor JR, Vaccarino F. 2004. Loss of glutamatergic pyramidal neurons in frontal and temporal cortex resulting from attenuation of FGFR1 signaling is associated with spontaneous hyperactivity in mice. J Neurosci. 24:2247–2258.

Shu Y, Hasenstaub A, Badoual M, Bal T, McCormick DA. 2003. Barrages of synaptic activity control the gain and sensitivity of cortical neurons. J Neurosci. 23:10388–10401.

Silbereis J, Cheng E, Ganat YM, Ment LR, Vaccarino FM. 2009. Precursors with glial fibrillary acidic protein promoter activity transiently generate GABA interneurons in the postnatal cerebellum. Stem Cells. 27:1152–1163.

Sohal VS, Zhang F, Yizhar O, Deisseroth K. 2009. Parvalbumin neurons and gamma rhythms enhance cortical circuit performance. Nature. 459:698–702.

Sowell ER, Kan E, Yoshii J, Thompson PM, Bansal R, Xu D, Toga AW, Peterson BS. 2008. Thinning of sensorimotor cortices in children with Tourette syndrome. Nat Neurosci. 11:637–639.

Sullivan EM, O'Donnell P. 2012. Inhibitory interneurons, oxidative stress, and schizophrenia. Schizophr Bull. 38:373–376.

Vicario-Abejon C, Collin C, McKay RD, Segal M. 1998. Neurotrophins induce formation of functional excitatory and inhibitory synapses between cultured hippocampal neurons. J Neurosci. 18:7256–7271.

Volk D, Austin M, Pierri J, Sampson A, Lewis D. 2001. GABA transporter-1 mRNA in the prefrontal cortex in schizophrenia: decreased expression in a subset of neurons. Am J Psychiatry. 158:256–265.

Volk DW, Austin MC, Pierri JN, Sampson AR, Lewis DA. 2000. Decreased glutamic acid decarboxylase67 messenger RNA expression in a subset of prefrontal cortical gamma-aminobutyric acid neurons in subjects with schizophrenia. Arch Gen Psychiatry. 57:237–245.

Wirth MJ, Brun A, Grabert J, Patz S, Wahle P. 2003. Accelerated dendritic development of rat cortical pyramidal cells and interneurons after biolistic transfection with BDNF and NT4/5. Development. 130:5827–5838.

Woo NH, Lu B. 2006. Regulation of cortical interneurons by neurotrophins: from development to cognitive disorders. Neuroscientist. 12:43–56.

Wuchter J, Beuter S, Treindl F, Herrmann T, Zeck G, Templin MF, Volkmer H. 2012. A comprehensive small interfering RNA screen identifies signaling pathways required for gephyrin clustering. J Neurosci. 32:14821–14834.

Wullner U, Isenmann S, Gleichmann M, Klockgether T, Bahr M. 1998. Expression of neurotrophins and neurotrophin receptors in the cerebellum of mutant weaver and lurcher mice. Brain Res Dev Brain Res. 110:1–6.

Xue M, Atallah BV, Scanziani M. 2014. Equalizing excitation-inhibition ratios across visual cortical neurons. Nature. 511:596–600.

Yamamoto J, Suh J, Takeuchi D, Tonegawa S. 2014. Successful execution of working memory linked to synchronized high-frequency gamma oscillations. Cell. 157:845–857.

Zheng K, An JJ, Yang F, Xu W, Xu ZQ, Wu J, Hokfelt TG, Fisahn A, Xu B, Lu B. 2011. TrkB signaling in parvalbumin-positive interneurons is critical for gamma-band network synchronization in hippocampus. Proc Natl Acad Sci USA. 108:17201–17206.